

## Green biogenic synthesis of silver nanoparticles: a thoroughly exploration of characterization and biological efficacy

N. Almasoud <sup>a</sup>, T. S. Alomar <sup>a</sup>, H. A. Aldehaish <sup>b</sup>, M. A. Awad <sup>c,\*</sup>,  
M. S. Alwahibi <sup>b</sup>, K. A. Alsalem <sup>d</sup>, S. Rai <sup>e,f</sup>, A. Bhattarai <sup>e</sup>, S. Almutlaq <sup>a</sup>,  
B. Alsudairi <sup>a</sup>, R. Alamr <sup>a</sup>, H. Alowais <sup>a</sup>

<sup>a</sup> Department of Chemistry, College of Science, Princess Nourah bint Abdulrahman University, P.O. Box 84427, Riyadh 11671, Saudi Arabia

<sup>b</sup> Department of Botany and Microbiology, King Saud University, Riyadh, Kingdom of Saudi Arabia

<sup>c</sup> King Abdullah Institute for Nanotechnology, King Saud University, Riyadh, 11451, Saudi Arabia

<sup>d</sup> College of Medicine, Imam Mohammad Ibn Saud Islamic University, Riyadh, Kingdom of Saudi Arabia

<sup>e</sup> National Archives, Ministry of Culture, Tourism and Civil Aviation, Government of Nepal, Kathmandu 44600, Nepal

<sup>f</sup> Department of Chemistry, Mahendra Morang Adarsh Multiple Campus, Tribhuvan University, Biratnagar, 56613, Nepal

Conventional physical and chemical methods for synthesizing silver nanoparticles (AgNPs) often use reducing agents, and other chemicals that are harmful to the environment because of their toxic properties. This has prompted significant concern and the need to develop environmentally acceptable approaches. Due to the constraints of traditional chemical-physical methods, green synthesis methods are being developed to fill these gaps by utilizing biological components extracted from plants. These plant-derived biomolecules are highly specific and facilitate the creation of metal nanoparticles. AgNPs, produced through these methods, possess a wide variety of metabolites with antibacterial effects. In light of this, the current investigation aimed to produce AgNPs using aqueous extracts obtained from *Moringa* leaves (MI), *Juniper* leaves (JI), and *Juniper* beans (Jb) via a green chemistry technique. Various analytical methods, including UV-visible spectrophotometry (UV-Vis), transmission electron microscopy (TEM), dynamic light scattering (DLS), Fourier transform infrared spectroscopy (FT-IR), and energy-dispersive X-ray spectroscopy (EDX) analysis, were employed to characterize the synthesized AgNPs. After adding the plant extracts, the color of the aqueous silver nitrate solution noticeably changed to brown. Furthermore, a shift in absorption spectra was noted, with absorbance peaks appearing around  $\lambda_{max} = 449.5$  nm, 478.5 nm, and 440.5 nm for Juniper leaves, Jb, and *Moringa* extracts, respectively. DLS analysis revealed that the synthesized AgNPs varied in size and polydispersity index (PDI) values, with sizes of 108 nm (PDI = 0.246), 101 nm (PDI = 0.278), and 161 nm (PDI = 0.240) from JI, Jb, and MI extracts, respectively. These nanoparticles displayed no agglomeration and were stable over a long period. Transmission electron microscope/TEM analysis confirmed the synthesis of well/dispersed AgNPs with an average sizes of less than 22 nm, displaying different shapes likely due to the variety of capping agents present in the bean and leaf extracts. Elemental profiles showed a peak at 3 keV for the synthesized AgNPs, indicating a high proportion of silver elements in all three samples. The synthesized nanoparticles were also subjected to biological screening. The investigation involved testing their antibacterial activity against various bacterial and fungal strains. The JInano extract exhibited significant antifungal activity. Conversely, the aqueous and nano-extracts of MI showed less effectiveness against fungal growth. The plant nano extracts, in particular, demonstrated a clearer effect against all tested fungi compared to the plant aqueous extracts. Among the AgNPs synthesized, those from *Moringa* extract had the greatest effect on Gram-positive bacteria (*S. aureus*), with an inhibitory zone diameter of 4.5 mm.

\* Corresponding author: mawad@ksu.edu.sa  
<https://doi.org/10.15251/DJNB.2024.194.1791>

(Received September 19, 2024; Accepted November 21, 2024)

Keywords: Analytical techniques, Antimicrobial, AgNPs, Green synthesis, Juniper leaves, Juniper beans, Moringa leaves

## 1. Introduction

Concerns around antimicrobial resistance are on the rise globally. The increasing number of antibiotic-resistant microorganisms challenges current and future medical advances. Therefore, researchers continually search for new, cost-effective, and more efficient therapeutic agents to combat microbial infections and eliminate bacterial resistance [1]. The increasing frequency of bacterial resistance causes substantial mortality and morbidity across the globe; as a result, the discovery of new antibacterial drugs is of crucial relevance [2]. Among the various nanoparticles utilized for these applications, metallic AgNPs are regarded as having the most promising antibacterial capabilities due to their high surface-to-volume ratio. Due to the rising prevalence of microbial resistance to metal ions and antibiotics, scientists have a vested interest in studying this characteristic. Many technological and environmental issues are looking to nanoparticles as a potential solution. The risks to international efforts are lessened by biological synthesis techniques for NPs [3].

Metallic nanoparticles (MNPs) have been reported as a potential substitute for antibacterial drugs, due to their effectiveness against bacteria and fungi [4-6]. MNPs exhibit greater physiological activity and require lower doses than their bulk metal equivalents due to their shape - size and high ratio of surface/volume [7]. Also, nanoparticles use many antimicrobial strategies, such as creating reactive oxygen species (ROS) that impair protein and RNA production and affect microbial membrane integrity. Nanoparticles also have unique physicochemical and biological properties, including the ability to fight tumors, inflammation, and bacteria.

AgNPs have recently attracted significant attention because of their distinctive antibacterial properties. Diagnostics, coatings, and sensors are just some of the many uses for silver nanomaterials. It has also been suggested that AgNPs may be an invaluable asset in the bioformulation of novel antimicrobial drugs, developing drug delivery formulations, and creating diagnostic and detection platforms. By penetrating the cell and interfering with essential processes at the cellular and subcellular levels, AgNPs stifle bacterial growth [3]. These characteristics allow a high level of interaction between the MNPs' surface and microbial membrane [8]. They can be produced using a range of physical-chemical methods, including thermal breakdown, sonication, electrochemistry, and chemical reduction [9-11]. The antifungal efficacy of green nanomaterials is greater than that of chemically synthesized nanomaterials<sup>2</sup>. Two of the main disadvantages that are associated with using these methods include high energy consumption and the use of potentially hazardous chemicals [12-14].

Synthesising AgNP through chemistry is a straightforward approach that produces high yields. The primary drawbacks of the chemical method to AgNP production are the high cost of synthesis and the different processes necessary to avoid particle aggregation. Furthermore, nanoparticles that are chemically manufactured release harmful byproducts into the environment. In addition, harmful chemical adsorption on nanoparticles occurs when a chemical approach is used for AgNP production, which has a detrimental effect when used [15]. On the other hand, green biosynthesis of nanomaterials has used less dangerous stabilizing and reducing agents, most notably plant extracts. Plant extracts are used in a natural reaction process that is not bound by extreme or stringent reaction conditions, which results in biogenic nanomaterials. Another benefit of green nanomaterials synthesized by plant extract is their reduced cytotoxicity [16].

Meanwhile, green nanotechnology is gaining popularity as a means of facilitating the production of nanoparticles that are environmentally friendly, safer for living beings, and possess sustainable commercial viability. Moreover, there has been an increase in demand to develop more ecologically material synthesis techniques, and the biosynthesis of nanoparticles, which connects biotechnology with nanotechnology, has drawn more attention. Moreover, the quest for suitable

biomaterials for the production of nanoparticles is still ongoing [7]. MNPs have also sparked interest in their "green synthesis" [18].

At present, plants or their extracts are commonly used to produce AgNPs. Various plant species, such as *Solanum xanthocarpum* L. Berry [19], tea leaves [20], *Callicarpa* mainly stem bark [21], *Trachyspermum ammi*, *Bauhinia variegata* [22], *Terminalia chebula* [23], and *Papaver somniferum* [24], have been utilized for this purpose. Furthermore, the use of other plants in producing AgNPs has also been reported, such as *Hevea brasiliensis* [25] and *Memecylon edule* [26]. However, the potential of such plants for nanoparticle synthesis is yet to be studied. This study used an eco-friendly green chemistry technique to synthesize AgNPs from extracts of *Moringa* leaves (*MI*), *Juniper* leaves (*JL*), and *Juniper* beans (*Jb*) as a reducing agents. *Moringa oleifera* is a wild herbaceous plant widely distributed throughout many tropical countries, including India. Its leaves contain active ingredients such as astragalins, cryptochlorogenic acid, and isoquercetin [27]. *Juniperus procera* is found naturally in Saudi Arabia and East Africa [28,29] and possesses many reported medical benefits, such as its anti-cancer, insecticidal, and antimicrobial properties [30-32]. The main goal of this study was to characterize the synthesis of AgNPs using various analytical techniques and evaluate their efficacy against different pathogen strains.

## 2. Materials and methods

### 2.1. Materials

The silver nitrate ( $\text{AgNO}_3$ , with a purity of over 99.99%) was sourced from Sigma Aldrich, the *MI* were collected from well-grown trees in farm that are located in Saudi Arabia in 2022, and the *JL* and beans were purchased from Amazon.

### 2.2. Plant extract preparation and silver nanoparticle synthesis (AgNPs)

The collected plants (*Moringa* leaves (*MI*), *Juniper* leaves (*JL*), and *Juniper* beans (*Jb*)) were cleaned, dried, and powdered into fine powder. Twenty grams of plant powder was soaked in 100 mL of boiled distilled water and left overnight. This was followed by filtration to isolate the *MI*, *JL*, and *Jb* aqueous extracts. The formulation of silver nanoparticles (AgNPs) was carried out by separately adding 10 mL of each *MI*, *JL*, and *Jb* aqueous extract to 1.0 mM silver nitrate ( $\text{AgNO}_3$ ) solutions. The reaction mixtures were then subjected to continuous stirring at 90°C to facilitate the formation of AgNPs. The produced AgNP samples were stored at ambient temperature and in complete darkness to prevent particle agglomeration. Figure 1 Shows a visual representation of the key stages and components involved in this synthesis method of green eco/synthesis of AgNPs using plant extracts. The visual observation during the synthesis process has been illustrated in Figure 2.

◆ Biomass as reducing, stabilizing and capping agents

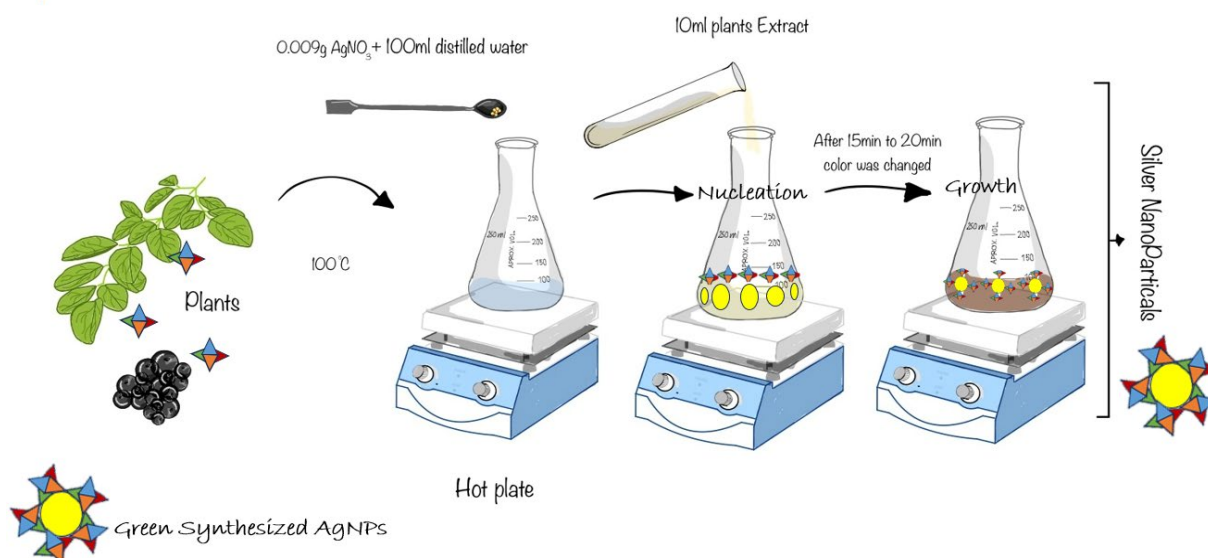


Fig. 1. Mechanistic of Green eco/synthesis of AgNPs using plants extracts.

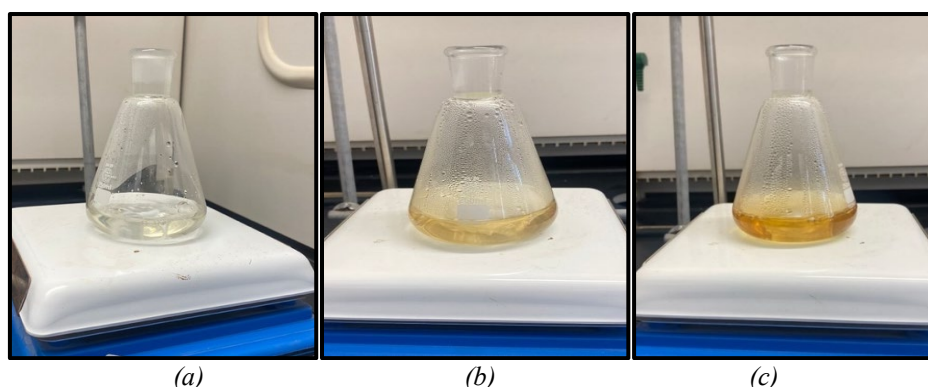


Fig. 2. Visual observation (A) silver nitrate solution (colorless), (B) 5 mins after adding plants extracts (a faded brown color appears), and (C) 15 mins after complete synthesis of AgNPs takes place (dark brown color).

### 2.3. Characterization of synthesized AgNPS

The optical properties of the synthesized AgNPs were examined using a UV -2450 Spectrophotometer from Shimadzu Corporation, Kyoto, Japan. Dynamic Light Scattering (DLS) was then performed utilizing a zeta sizer (Malvern, UK) to measure the size distribution of the AgNPs. This was followed by the use of Fourier Transform Infrared Spectroscopy (FT-IR) on a Spectrum BX spectrometer from PerkinElmer, Waltham, U.S.A., within the wave number range of 4000-400 cm<sup>-1</sup>, to identify the functional groups present in the samples.

The surface morphology and resulting nanoparticle sizes were analyzed using transmission electron microscopy (TEM, JEM-2100F, JEOL Ltd, USA) at an accelerating voltage of 200 kV. The presence of silver in the suspension was confirmed through energy dispersive X-ray spectroscopy (EDX) analysis, which also detected other core particle components.

### 2.4. Antimicrobial assignment

The plates were incubated overnight with the following bacterial strains: *Escherichia coli* (*E.coli*) and *Pseudomonas aeruginosa* (*P. aeruginosa*) (Gram-negative), and *Staphylococcus aureus* (*S. aureus*) and *Bacillus subtilis* (*B. subtilis*) (Gram-positive), obtained from the Botany and

Microbiology Department, King Saud University (KSU). The synthesized Ag-NPs and the aqueous extract from the plant species used in the study were steadily aliquoted until the wells were filled. The combined substances were then mixed and incubated at 37 degrees Celsius for a full day. After that, the damping zone's diameter was computed.

### 2.5. Antifungal assignment

The antifungal activity of the samples in four fungi was studied: *Alternaria alternata*, *Trichoderma stromatic*, and *Fusarium solani*. These samples were obtained from Botany and Microbiology Department at King Saud University. PDA media was then prepared and sterilized. This was followed by mixing 2 ml of treatment was added to 20 ml of PDA media in a Petri dish, and the mixture was homogenized. This was followed by transferring a disc of fungi, using an inoculation needle, and placing it upside down in the middle of the dish. The party dish containing the samples was then incubated at 27 °C for 5 days. The Petri dishes containing the samples were incubated at 27 °C for 5 days. The results were photographed using a digital camera (Canon PowerShot ELPH 180- 20MP, Japan) The diameter of the fungal growth was measured from the plate directly using a ruler. The results were recorded and compared to the control experiment (non-nano plant extract).

## 3. Results and discussion

### 3.1. UV–Vis spectroscopy analysis of AgNPs

Subsequently visually inspecting the progress of silver ion ( $\text{Ag}^+$ ) reduction to G-AgNPs, the reaction media was scanned at regular intervals using UV-Vis spectroscopy. Upon adding the aqueous plant extract to the  $\text{AgNO}_3$  solution, the color visibly changed from yellow to brown (Figure 2) was observed. One research study showed that Plant extract metabolites converted silver ( $\text{Ag}^+$ ) ions to silver (Ag) atoms ( $\text{Ag}^0$ ) [34]. Surface plasmon vibrations (SPR) in the resultant AgNPs were excited as a consequence of the decrease, causing an absorbance peak that appears around  $\lambda_{\text{max}}=449.5, 478.5, \text{ and } 440.5\text{nm}$  for *Jl*, *Jb*, and *Ml* extracts, respectively as a result of the excitation of the SPR in the AgNPs [35]. Since Surface plasmon vibrations (SPR) depends on a number of characteristics, including particle size and/or the dielectric constant of the surrounding medium, it is often employed as an indicative tool for metal nanoparticle production. Extracellular reduction of  $\text{Ag}^+$  ions suggests the creation of Ag nanoparticles [36]

The sharp UV-Vis absorption spectra of AgNPs produced by *Jl*, *Jb*, and *Ml* extracts are shown in Figure 3 (A-C), commonly measured between 350 and 600 nm for colloidal silver nanoparticles [37]. As a result of size and shape differences, as well as other physical features, produced silver nanoparticles (AgNPs) exhibit varying UV spectra [38].

Other studies [39] stated that; silver NPs in the reaction fluid had spectra with an absorption peak at 430-450 nm, whereas they claimed that the peak absorbance occurs at 438 nm. The phytochemical's presence on the AgNPs' surface, which assists in capping, was also identified, as indicated by peaks not before mapped.

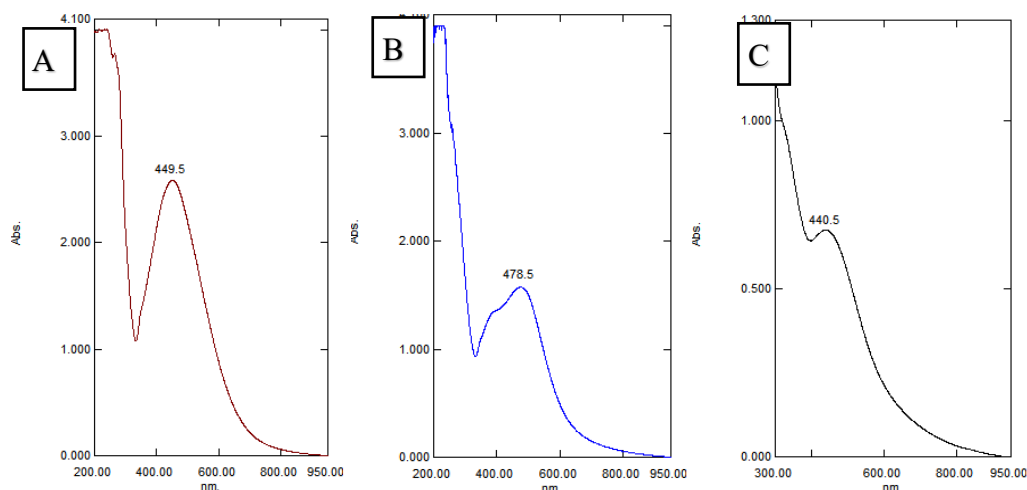


Fig. 3. The UV-Vis absorption spectra of the synthesized AgNPs using (A) *Jl*, (B) *Jb*, and (C) *Ml* extracts, respectively.

### 3.2. DLS analysis of AgNPs

DLS is one of the greatest adaptable methods for measuring NP size, size distribution, hydrodynamic diameter, and stabilization [40-42]. DLS analysis provided the average zeta diameter (nm) of the resulting AgNPs. In an aqueous solution containing a metallic core, ions, and biological macromolecules attached to the surface of NP, the DLS method is used to assess the hydrodynamics of NP size [43]. Figure 4 shows the mean average sizes and polydispersity indices (Pdl) of the AgNP suspensions. Size populations within a specific sample are represented by Pdl. The particle size distribution index (Polydispersity index, PDI) reflects on a value between 0.0 (representing a fully monodisperse sample) and 1.0 (representing a substantially poly-disperse sample with numerous particle size populations). According to a research [44] values of 0.2 or less are generally considered acceptable in practise for NPs materials. Therefore, the synthesized AgNPs differed in size, displayed no agglomeration, and were stable for a long time. Furthermore, the data was collated in Table 1.

Table 1. Mean average size and polydispersity index (Pdl) of the synthesized AgNPs.

Samples	Size (nm)	Pdl
<i>Jl</i> -AgNPs	108	0.246
<i>Jb</i> -AgNPs	161	0.240
<i>Ml</i> -AgNPs	101	0.278

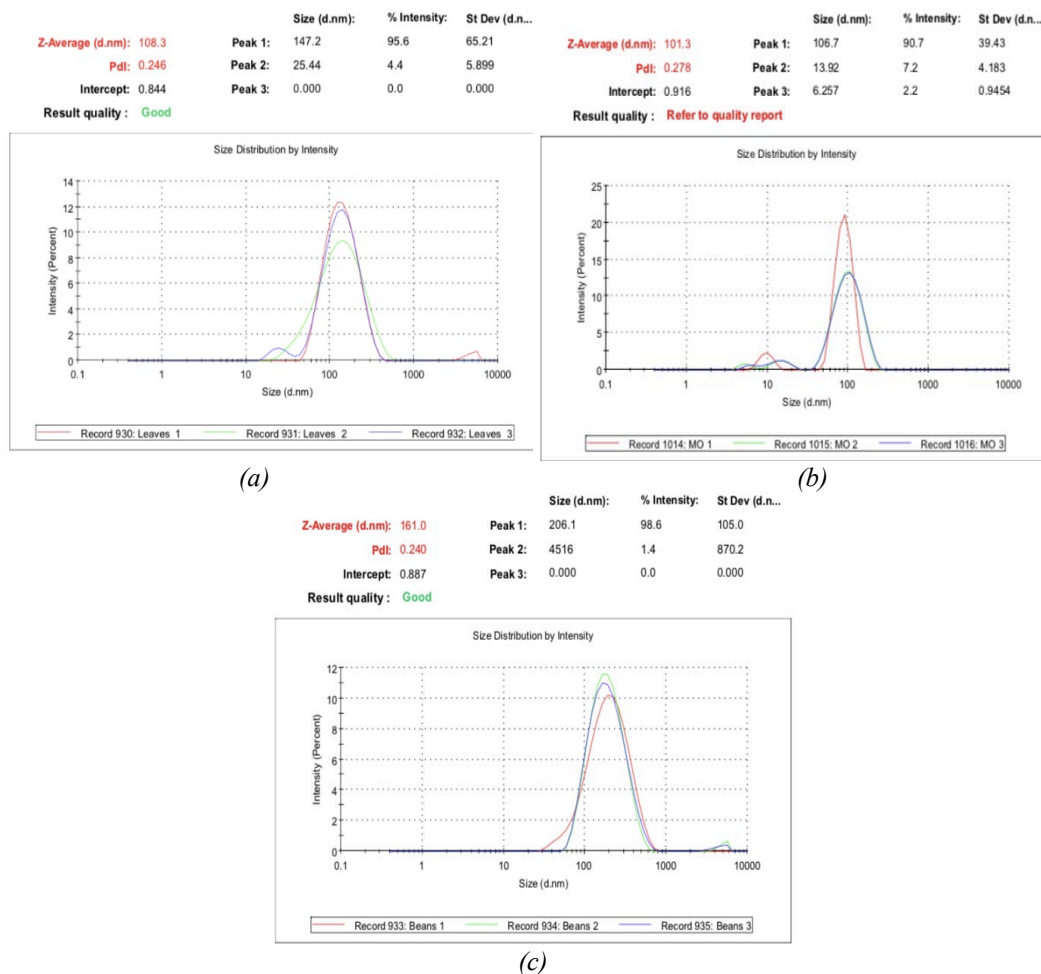


Fig. 4. Zeta size of synthesized AgNPs using (A) *Jl*, (B) *Jb*, and (C) *ML*, respectively.

### 3.3. TEM imaging and EDX spectra analysis of AgNPs

TEM and EDX analysis were achieved to define the particle magnitude, shape, morphology, and elemental composition of the synthesized AgNPs. Electron micrographs of the synthesized sample clearly showed the nanoparticles because of their high resolution, so the resolution will not be affected by the remaining formulation. Minor differences in particle shapes and morphologies were detected between samples of Ag NPs synthesized by *Jl*, *Jb*, and *ML* extracts (Figure 5 (A, B, and C)). In particular, as shown in Figures 5A and 5C, the majority of particles were found to be polydispersed and spherical. In contrast, Figure 5B showed that the particles appeared elongated and well-dispersed, spherical particles of various sizes with little agglomeration. All in all, the morphology of the synthesized AgNPs varied, possibly due to various capping agents present in bean and leaf extracts [45,46].

EDX report provides qualitative and quantitative data about the elements that contribute towards the formation of nanoparticles. The elemental profiles for the synthesized AgNPs indicated a higher count at 3 keV, resulting in a large proportion of silver elements in all three samples (Figure 5(D, E, and F)). This confirmed the formation of AgNPs since it often exhibits an optical absorption peak around 3 keV attributed to the (SPR) surface plasmon resonance [47,48]. Further, EDX analysis verified the presence of carbon(C), oxygen (O<sub>2</sub>), potassium (K), and chlorine (Cl) in the three synthesized AgNP samples. In addition, the *Jl*-AgNPs and *ML*-AgNPs samples contained sodium (Na) (Figures 5 (D and F)), while *Jb*-AgNPs contained calcium(Ca) (Figure 5E). Aluminum (Al) was reported only in *ML*-AgNPs (Figure 5F).

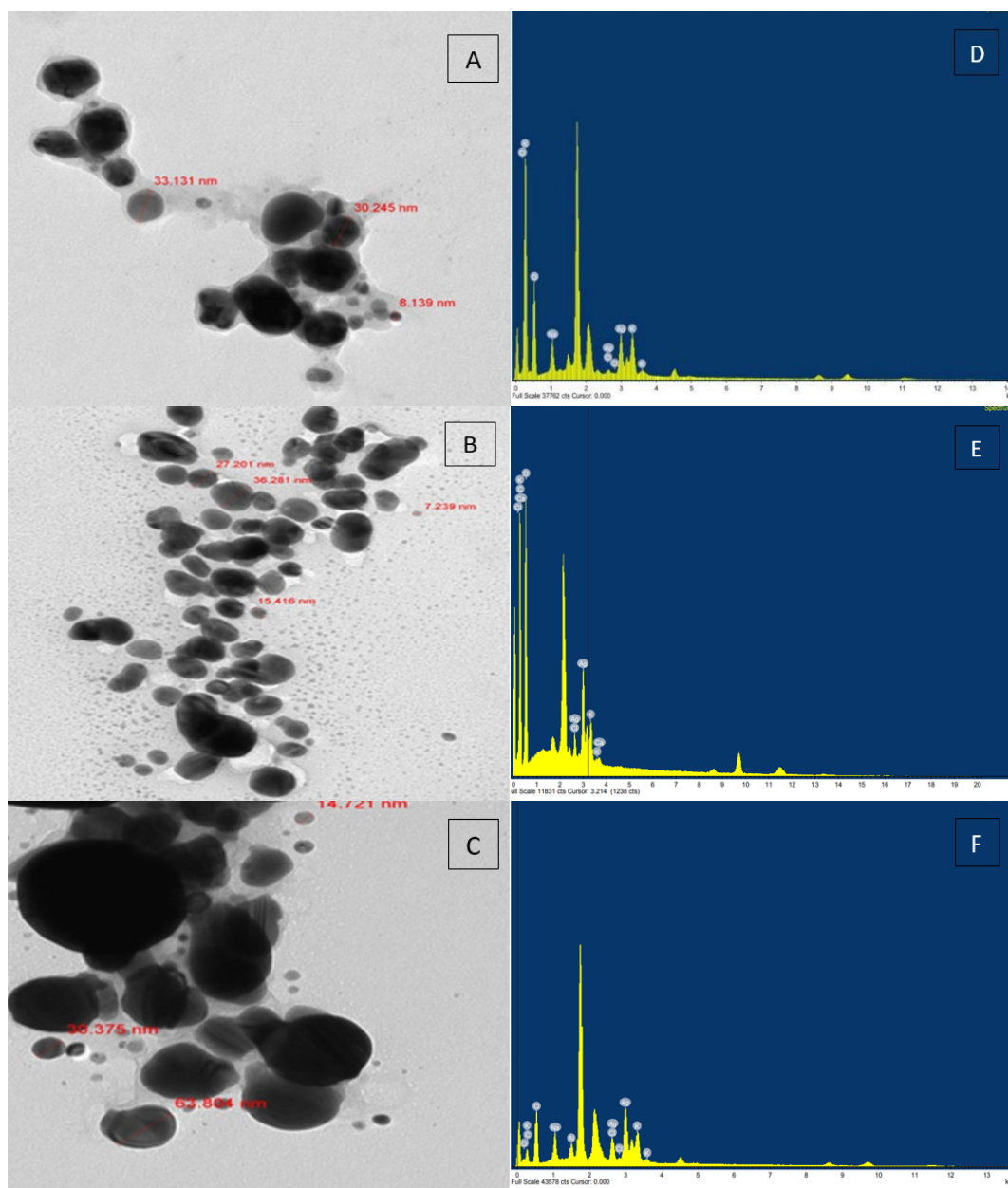


Fig. 5. TEM micrographs and elements analysis spectra of the synthesized AgNPs using (A) Juniper leaves, (B) *Jb*, and (C) *Ml* extracts, respectively.

### 3.4. FT-IR analysis of Ag-nanoparticles

The analysis of samples using FT-IR spectroscopy indicated that functional groups in the plant extracts are responsible for the reduction and stability of the formed Ag-nanoparticles. Figure 6 shows the FT-IR spectra of the *Jl*, *Jb*, and *Ml* aqueous extracts and the synthesized AgNPs from the respective extracts.

Figure 6 (A and B) show the spectra for *Jl* extract and synthesized *Jl*-AgNPs; both spectra exhibited identical peaks with only a slight shift at  $3427.97\text{cm}^{-1}$  and  $3429.49\text{cm}^{-1}$ . Identical spectra were recorded for *Jb* extracts, and the synthesized AgNPs also exhibited a slight shift at  $3398.13\text{cm}^{-1}$  and  $3396.05\text{cm}^{-1}$  (Figure 6 (C and D)). These bands corresponded to O-H stretching groups (phenols, alcohols) or N-H functional groups (amides or amines). The hydroxyl (–OH) groups played a key role in reducing  $\text{Ag}^+$  ions to form Ag nanoparticles. The change in peak locations suggested that the synthesized AgNPs were highly reductive and stable [47–49]. The peaks at

2931.69  $\text{cm}^{-1}$  and 3932.78  $\text{cm}^{-1}$  in the spectra of the *Jl* extracts and their *Jl*-AgNPs were assigned to CH-stretching region, the peaks around 1634.78  $\text{cm}^{-1}$  and 1633.67  $\text{cm}^{-1}$  were attributed to the C - O group (carboxylic acid), and the peaks at 1384.90  $\text{cm}^{-1}$  and 1404.31  $\text{cm}^{-1}$  were associated with the C-C group (alkenes).

Furtumore, for *Jb* extract, and its *Jb*-AgNPs, the peak around 2935.99  $\text{cm}^{-1}$  and 2936.04  $\text{cm}^{-1}$  corresponded to CH-stretching, at 1636.88  $\text{cm}^{-1}$  and 1636.28  $\text{cm}^{-1}$  to the C=C (alkenes), and at 1414.63  $\text{cm}^{-1}$  and 1385.23  $\text{cm}^{-1}$  to the bending of C-H bonds in alkanes. In Figure 6 (E and F), the 3409.46  $\text{cm}^{-1}$  and 3391.60  $\text{cm}^{-1}$  peaks corresponded to OH stretching groups. It was reported that the extract's biomolecules also exhibit a strong affinity for binding metal, showing the formation of a capping layer over metal NPs to avoid agglomeration and provide stability in the medium [50].

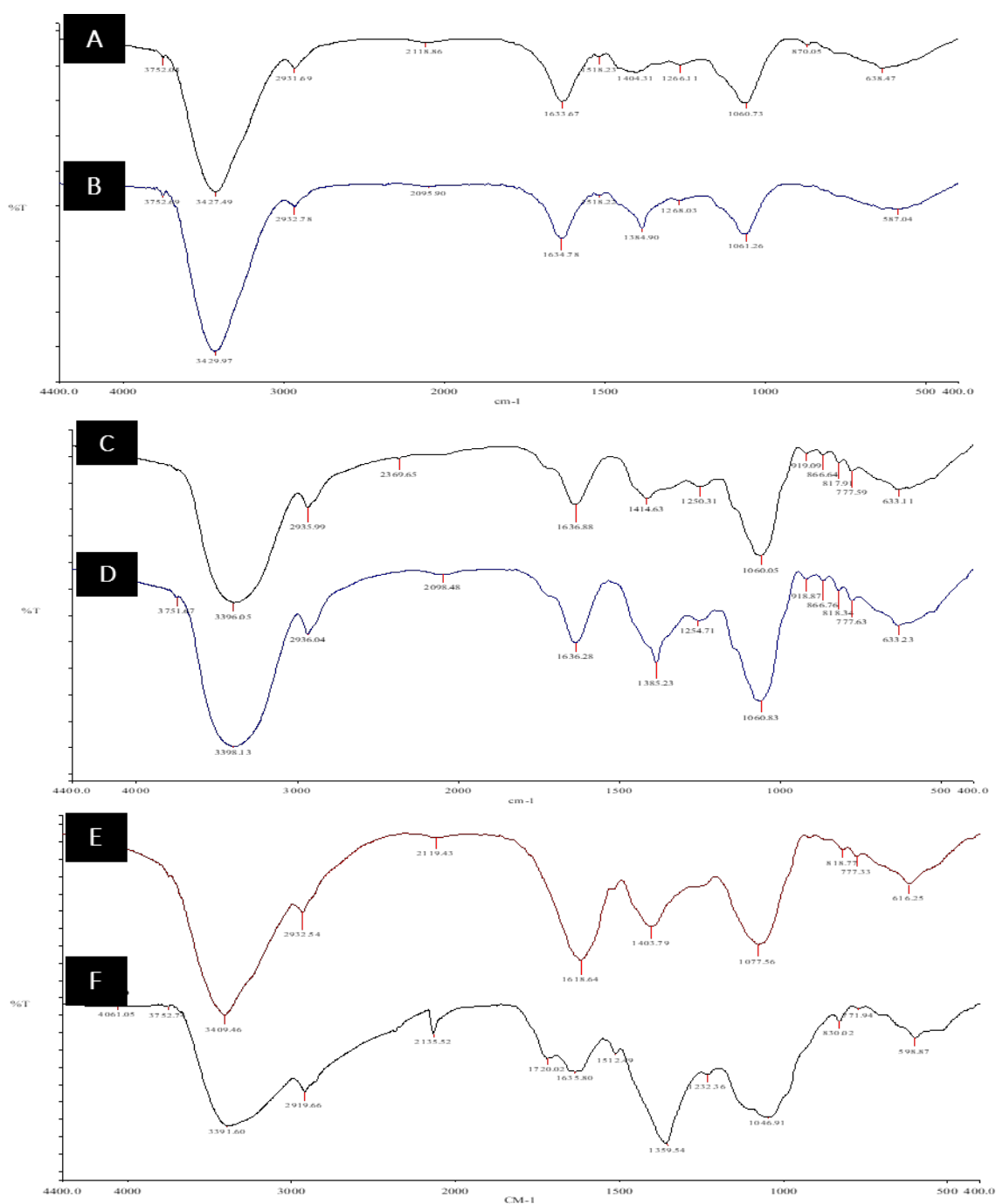


Fig. 6. FT-IR spectra of the aqueous plant extracts and green synthesized AgNPs: (A) *Jl* extract (*Jl*), (B) *Jl*-AgNPs (*JlN*), (C) *Jb* extract (*Jb*), (D) *Jb*-AgNPs (*JbN*), (E) *Ml* extract (*Mo*), and (F) *Ml*-AgNPs (*MoN*).

### 3.5. Biological Activity of AgNPs

#### 3.5.1. Assessment of Anti-bacterial activity

Results obtained from the antibacterial study indicated that the aqueous solution and nano plant extracts affected bacterial growth. The diameter measurement of the inhibition zone is correlated with the efficiency of the treated extract; there is an inverse relationship between the inhibition zone diameter and the microbe's resistance ability [51].

As shown in Table 2 and Figure 7 (A), the *Ml*-AgNPs sample had the greatest effect on positive bacteria (*S. aureus*) with an inhibitory zone diameter of 4.5 mm. The mechanism of action of silver is based on the interaction between thiol group molecules and the respiratory enzymes within bacterial cells. Ag nanoparticles coating the cell wall and membrane impede the respiratory process of the bacteria [51].

In depth analysis of *Jb*-AgNPs sample, indicated the presence of an inhibitory zone of diameter 3.1 mm on *S. aureus* and *P. aeruginosa* (Figure 7 (C)). The *Jl*-AgNPs showed an effect on the negative bacteria (*E. coli* and *P. aeruginosa*) with an inhibition zone of diameter 2.5 and 2.3 mm, respectively (Figure 7 (B)). Unlike gram-positive bacteria, which possess a thick peptidoglycan layer composed of linear polysaccharide chains linked by short peptides, gram-negative bacteria have a much thinner peptidoglycan layer. Due to their rigid structure, AgNPs are unable to penetrate the bacterial cell wall [52].

Hence, the effect on Gramnegative bacteria is more significant (noticeable) than on Grampositive bacteria. While some extracts appeared to have no significant impact on the tested microbes. Moreover, the nano-extracts were the most effective in treating resistant microbes in this study. This observation emphasizes the role of silver nanoparticles inhibit bacterial growth because the smaller particles have a greater surface area and release silver ions more quickly [53]. This is also because silver nanoparticles attract negatively charged bacteria via electrostatic interactions with their cell membranes due to their positive charge [54]. AgNPs are able to interface with cell membranes more efficiently than bulk metallic equivalents because of their high surface/volume ratio. In this way, AgNPs disrupt metabolic activity—such as the respiratory chain, DNA replication, and protein synthesis—by interacting with the sulfur/thiol and phosphorus components of proteins or DNA, ultimately resulting in cell death.

In the same way, it eliminates bacteria by inducing the production of reactive oxygen species (ROS), which oxidize the phospholipids in the cell wall. This process leads to the rupture of the membrane and the denaturation of proteins, RNA, and DNA within the cell [55]. Previous research has suggested several possible pathways for the antibacterial action of Ag-NPs. It has been recommended that Ag-NPs' antimicrobial effects against bacteria can be explained by (a) oxidative stress carried on by Ag-NPs' association with enzymes and other biomolecules; b) membrane disruption brought on by Ag-NPs' association/interaction with DNA and other biomolecules; c) suppression of cell multiplication [40].

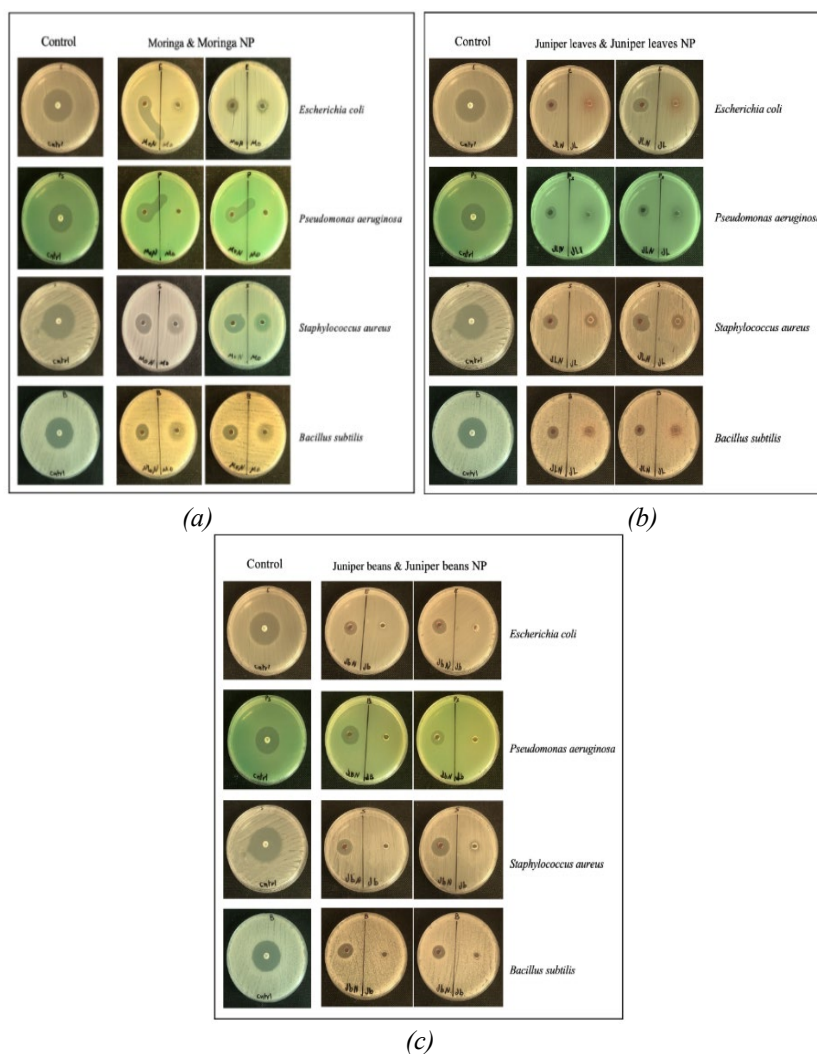


Fig. 7. Effect of (A) Ml, (B) Jl, and (C) Jb aqueous extracts and NPs samples on four types of bacteria.

Table 2 Effect of (A) Ml, (B) Jl, and (C) Jb aqueous extracts and NPs samples on four types of bacteria

Microbe species	Diameter of Inhibition zone (mm)						
	Control	Mo	Ml-AgNPs	Jl	Jl-AgNPs	Jb	Jb-Ag NPs
<i>E. coli</i>	9.6	1.1	1.5	0.4	2.5	0	2.3
<i>P. aeruginosa</i>	5.7	0	1.3	0	2.3	0	3.1
<i>S. aureus</i>	9.6	0	4.5	1.3	1.8	0.6	3.1
<i>B. subtilis</i>	7.1	0	2	0	1.1	0	1.8

Table 3. Antibacterial activity of the plant extracts and the synthesized AgNPs.

Extract	Fungus Diameter (cm)		
	<i>A. alternata</i>	<i>T. stromaticum</i>	<i>F. solani</i>
Control	9	9	9
<i>Ml</i> extract	4.6	9	4.6
<i>Ml</i> -AgNPs	6.9	9	4.5
<i>Jb</i> extract	6.5	9	4
<i>Jb</i> -AgNPs	0.9	1	1.6
<i>Jl</i> extract	6.6	9	4.2
<i>Jl</i> -AgNPs	1.5	1.9	2.5

Mo=*Moringa* extract, Jl= *Juniper* leaves extract, Jb= *Juniper* beans extract.

### 3.5.2. Antifungal activity

The extent of antifungal activity depends on the size of fungal growth on the nutrient media surface. The antifungal activity of the plant extracts and the synthesized AgNPs are tabulated in Table 3 and shown in Figure 8. Remarkably, the synthesized AgNPs samples from plants extracts exhibited a distinct effect against the fungi by interfering with internal cellular processes such as protein and DNA production. *Jl*-AgNPs exhibited significant activity, hindering fungal growth (Figure 8 (B)) [56]. On the other hand, both the aqueous extract of *Ml* and *Ml*-AgNPs showed comparatively lower effectiveness against fungal growth (Figure 8 (A)).

Among the tested samples, *Jb*-AgNPs showed a higher ability to resist the growth of all studied fungi, which was demonstrated through the fungal growth volume readings were 0.9, 1, and 1.6 cm for *A. alternata*, *T. stromaticum*, and *F. solani*, respectively (Figure 8 (C)). Furthermore, the *Jl*-AgNPs, which showed great activity against the growth of fungi (Figure 8 (B)). Both the aqueous extract of *Ml* and *Ml*-AgNPs showed less effectiveness against fungal growth (Figures 8 (A)). This may be due to the lack of active antifungal chemicals.

Various factors such as morphology, surface charge, Ag-NPs tolerance ability, sensitivity, type, sex, microbe species, NPs concentration, and time of allergen exposure all impact the antimicrobial effectiveness of Ag-NPs [57]. The extent to which AgNPs have antifungal efficacy against pathogenic fungi is largely unknown. Antifungal activity against *T. mentagrophytes* and other *Candida* species (including *C. albicans*, *C. tropical*, *C. glabrata*, *C. parapsilosis*, and *C. krusei*) was observed, however, suggesting the potential use of these nanoparticles. AgNPs severely damage the structure of fungal cell wall [10]. Shape, size, and surface charge have all been identified as contributors to Ag-NPs' antibacterial activity, Ag-NPs tolerance, species-sensitivity, bacterial type, genus, and species, NPs concentration, and exposure time all have a role. The findings demonstrated AgNPs' potential to inhibit plate-borne fungus growth. AgNPs are thought to prevent spores from developing by generating holes in the membrane of fungal cells, which may result in cell death. It has been hypothesized that free radical production, membrane damage, and pit development on the bacterial cell wall membrane are the mechanisms by which AgNP exerts its antibacterial effect (Figure 9). In addition, free radicals may disrupt the DNA and protein structure [40].

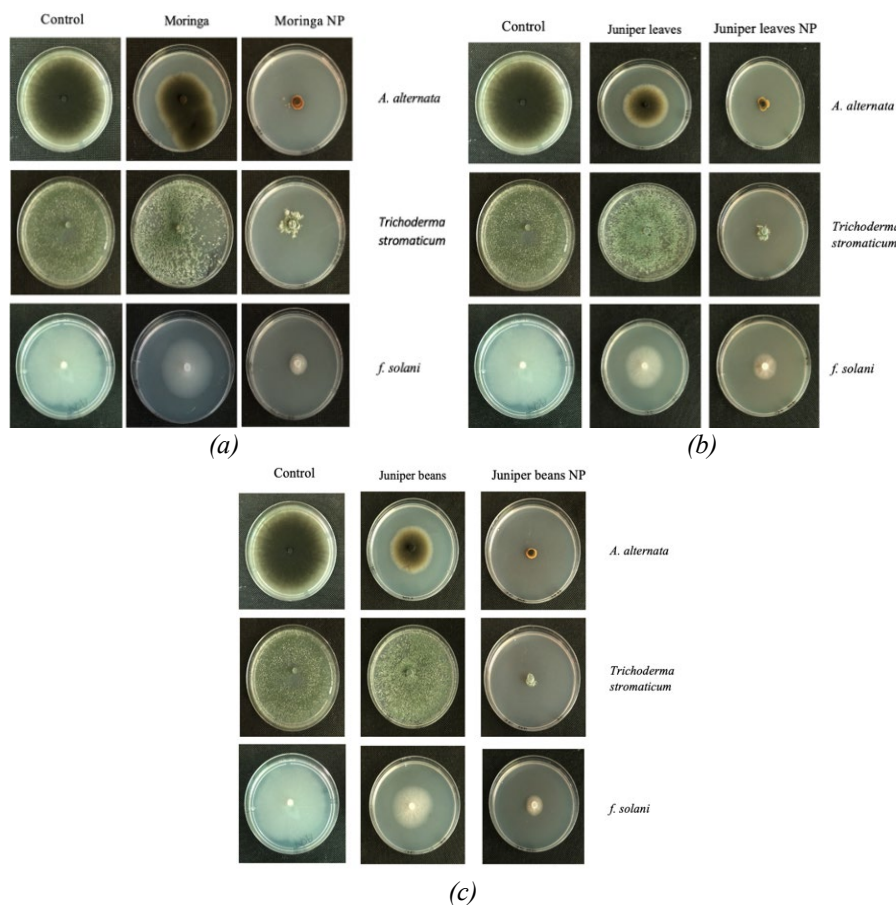


Fig. 8. Antifungal activity of the (A) *Ml*, (B) *Juniper leaves*, (C) *Jb* extracts, and formed AgNPs.

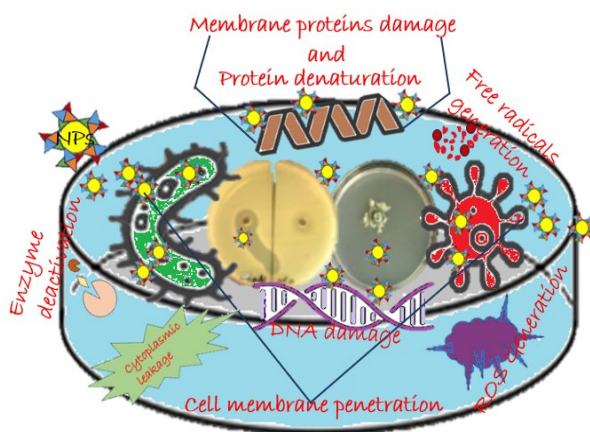


Fig. 9. The graph represents the possible mechanisms AgNPs strategies for antimicrobial activities.

#### 4. Conclusion

This work examined the feasibility of a green, eco-friendly approach for synthesizing silver nanoparticles (AgNPs) using aqueous extracts from *Moringa leaves*, *Juniper leaves*, and *Juniper beans*. Besides evaluating their biomedical applications, the nanoparticles were characterized using various analytical techniques including: UV-Vis, DLS, TEM, EDX, and FT-IR. TEM analysis revealed the synthesis of well-dispersed AgNPs with a variety of sizes and morphologies. DLS

analysis showed that the synthesized AgNPs varied in size, with diameters of 108 nm (PDI = 0.246), 101 nm (PDI = 0.278), and 161 nm (PDI = 0.240) for *Jl*, *Jb*, and *Ml* extracts, respectively. These nanoparticles displayed no agglomeration and were stable over a long period. The biological activity of the synthesized AgNPs was tested using numerous bacteria and fungi. The *Jlnano* extract demonstrated significant antifungal activity, whereas the aqueous and nano-extracts of *Ml* were less effective against fungal growth. Notably, the plant nano extracts showed a clearer effect against all tested fungi compared to the plant aqueous extracts. Furthermore, antibacterial activity data revealed that green-synthesized AgNPs were more effective against diverse types of microorganisms. These findings open up new possibilities for utilizing the synthesized AgNPs in various sectors, including pharmaceuticals, cosmetics, biomedicine, and nanomedicine.

### Conflicts of interest

The authors declare no conflict of interest.

### Acknowledgements

The authors extend their appreciation to the Deputyship for Research & Innovation, Ministry of Education in Saudi Arabia for funding this research work through the project number RI-44-0371.

### References

- [1] A. U. Rahman, A. U. Khan, Q. Yuan, Y. Wei, A. Ahmad, S. Ullah, Z. U. H. Khan, S. Shams, M. Tariq, W. Ahmad, *Journal of Photochemistry and Photobiology B: Biology*, 2019, 193, 31-38; <https://doi.org/10.1016/j.jphotobiol.2019.01.018>
- [2] M. T. Yassin, A. A.-F. Mostafa, A. A. Al-Askar, F. O. Al-Otibi, *Crystals*, 2022, 12, 603; <https://doi.org/10.3390/cryst12050603>
- [3] P. Mathur, S. Jha, S. Ramteke, N. Jain, *Artificial cells, nanomedicine, and biotechnology*, 2018, 46, 115-126; <https://doi.org/10.1080/21691401.2017.1414825>
- [4] J. Quek, E. Uroro, N. Goswami, K. Vasilev, *Materials Today Chemistry*, 2022, 23, 100606; <https://doi.org/10.1016/j.mtchem.2021.100606>
- [5] B. Sahin, R. Aydin, S. Soylu, M. Türkmen, M. Kara, A. Akkaya, H. Çetin, E. Ayyıldız, *Inorganic Chemistry Communications*, 2022, 135; <https://doi.org/10.1016/j.inoche.2021.109088>
- [6] A. H. Abbas, N. Y. Fairouz, *Materials Today: Proceedings*, 2022, 61, 908-913; <https://doi.org/10.1016/j.matpr.2021.09.551>
- [7] A. Nieto-Maldonado, S. Bustos-Guadarrama, H. Espinoza-Gomez, L. Z. Flores-López, K. Ramirez-Acosta, G. Alonso-Nuñez, R. D. Cadena-Nava, *Journal of Environmental Chemical Engineering*, 2022, 10, 107130; <https://doi.org/10.1016/j.jece.2022.107130>
- [8] P. Sharma, S. Pant, V. Dave, K. Tak, V. Sadhu, K. R. Reddy, *Journal of microbiological methods*, 2019, 160, 107-116; <https://doi.org/10.1016/j.mimet.2019.03.007>
- [9] S. K. Das, E. Marsili, *Bioinspired metal nanoparticle: synthesis, properties and application*, Croacia: InTech, 2011.
- [10] S. Rajeshkumar, S. Menon, S. V. Kumar, M. M. Tambuwala, H. A. Bakshi, M. Mehta, S. Satija, G. Gupta, D. K. Chellappan, L. Thangavelu, *Journal of Photochemistry and Photobiology B: Biology*, 2019, 197, 111531; <https://doi.org/10.1016/j.jphotobiol.2019.111531>
- [11] P. Yugandhar, T. Vasavi, P. Uma Maheswari Devi, N. Savithamma, *Applied Nanoscience*, 2017, 7, 417-427; <https://doi.org/10.1007/s13204-017-0584-9>

- [12] J. Suárez-Cerda, H. Espinoza-Gómez, G. Alonso-Núñez, I. A. Rivero, Y. Gochi-Ponce, L. Z. Flores-López, *Journal of Saudi Chemical Society*, 2017, 21, 341-348; <https://doi.org/10.1016/j.jscs.2016.10.005>
- [13] M. A. Asghar, E. Zahir, S. M. Shahid, M. N. Khan, M. A. Asghar, J. Iqbal, G. Walker, *Lwt*, 2018, 90, 98-107; <https://doi.org/10.1016/j.lwt.2017.12.009>
- [14] H. Espinoza-Gómez, L. Z. Flores-López, K. A. Espinoza, G. Alonso-Núñez, *Applied Nanoscience*, 2020, 10, 127-140; <https://doi.org/10.1007/s13204-019-01070-w>
- [15] V. Soni, P. Raizada, P. Singh, H. N. Cuong, S. Rangabhashiyam, A. Saini, R. V. Saini, Q. Van Le, A. K. Nadda, T.-T. Le, *Environmental Research*, 2021, 202, 111622; <https://doi.org/10.1016/j.envres.2021.111622>
- [16] N. Shreyash, S. Bajpai, M. A. Khan, Y. Vijay, S. K. Tiwary, M. Sonker, *ACS Applied Nano Materials*, 2021, 4, 11428-11457; <https://doi.org/10.1021/acsanm.1c02946>
- [17] K. Shameli, M. B. Ahmad, A. Zamanian, P. Sangpour, P. Shabanzadeh, Y. Abdollahi M. Zargar, *International journal of nanomedicine*, 2012, 7, 5603; <https://doi.org/10.2147/IJN.S36786>
- [18] P. K. Dikshit, J. Kumar, A. K. Das, S. Sadhu, S. Sharma, S. Singh, P. K. Gupta, B. S. Kim, *Catalysts*, 2021, 11, 902; <https://doi.org/10.3390/catal11080902>
- [19] M. Amin, F. Anwar, M. R. S. A. Janjua, M. A. Iqbal, U. Rashid, *International Journal of Molecular Sciences*, 2012, 13, 9923-9941; <https://doi.org/10.3390/ijms13089923>
- [20] Y. Y. Loo, B. W. Chieng, M. Nishibuchi, S. Radu, *International journal of nanomedicine*, 2012, 7, 4263.
- [21] K. Shameli, M. Bin Ahmad, E. A. Jaffar Al-Mulla, N. A. Ibrahim, P. Shabanzadeh, A. Rustaiyan, Y. Abdollahi, S. Bagheri, S. Abdolmohammadi, M. S. Usman, *Molecules*, 2012, 17, 8506-8517; <https://doi.org/10.3390/molecules17078506>
- [22] V. Kumar, S. Yadav, *IET nanobiotechnology*, 2012, 6, 1-8; <https://doi.org/10.1049/iet-nbt.2010.0015>
- [23] K. M. Kumar, M. Sinha, B. K. Mandal, A. R. Ghosh, K. S. Kumar, P. S. Reddy, *Spectrochimica Acta Part A: Molecular and Biomolecular Spectroscopy*, 2012, 91, 228-233; <https://doi.org/10.1016/j.saa.2012.02.001>
- [24] K. Vijayaraghavan, S. K. Nalini, N. U. Prakash, D. Madhankumar, *Colloids and Surfaces B: Biointerfaces*, 2012, 94, 114-117; <https://doi.org/10.1016/j.colsurfb.2012.01.026>
- [25] E. J. Guidelli, A. P. Ramos, M. E. D. Zaniquelli, O. Baffa, *Spectrochimica Acta Part A: Molecular and Biomolecular Spectroscopy*, 2011, 82, 140-145; <https://doi.org/10.1016/j.saa.2011.07.024>
- [26] T. Elavazhagan, K. D. Arunachalam, *International Journal of Nanomedicine*, 2011, 6, 1265; <https://doi.org/10.2147/IJN.S18347>
- [27] J. Fernandez, R. Reyes, H. Ponce, M. Oropeza, M.-R. VanCalsteren, C. Jankowski, M. G. Campos, *European Journal of Pharmacology*, 2005, 522, 108-115; <https://doi.org/10.1016/j.ejphar.2005.08.046>
- [28] R. P. Adams, *Biochemical systematics and ecology*, 1990, 18, 207-210; [https://doi.org/10.1016/0305-1978\(90\)90061-J](https://doi.org/10.1016/0305-1978(90)90061-J)
- [29] M. Van Slageren, *Kew Bulletin*, 2001, 56, 1021; <https://doi.org/10.2307/4119320>
- [30] T. Abdel Ghany, O. M. Hakamy, *J. Biol. Chem. Res*, 2014, 31, 668-677.
- [31] I. Tumen, F. J. Eller, C. A. Clausen, J. A. Teel, *BioResources*, 2013, 8, 12-20; <https://doi.org/10.15376/biores.8.1.12-20>
32. D. Bitew, *J Plant Pathol Microb*, 2015, 6, 2.
- [33] V. Vidhu, S. A. Aromal, D. Philip, *Spectrochimica Acta Part A: Molecular and Biomolecular Spectroscopy*, 2011, 83, 392-397; <https://doi.org/10.1016/j.saa.2011.08.051>
- [34] N. Pantidos, L. E. Horsfall, *Journal of Nanomedicine & Nanotechnology*, 2014, 5, 1.
- [35] O. Erdogan, M. Abbak, G. M. Demirbolat, F. Birtekocak, M. Aksel, S. Pasa, O. Cevik, *PLoS one*, 2019, 14, e0216496; <https://doi.org/10.1371/journal.pone.0216496>

- [36] M. Naveed, B. Bukhari, T. Aziz, S. Zaib, M. A. Mansoor, A. A. Khan, M. Shahzad, A. S. Dabool, M. W. Alruways, A. A. Almalki, *Molecules*, 2022, 27, 4226; <https://doi.org/10.3390/molecules27134226>
- [37] M. S. Jabir, A. A. Hussien, G. M. Sulaiman, N. Y. Yaseen, Y. H. Dewir, M. S. Alwahibi, D. A. Soliman, H. Rizwana, *Artificial cells, nanomedicine, and biotechnology*, 2021, 49, 48-60; <https://doi.org/10.1080/21691401.2020.1867152>
- [38] H. M. Abdelmigid, M. M. Morsi, N. A. Hussien, A. A. Alyamani, N. M. Al Sufyani, *Journal of nanomaterials*, 2021, 2021, 1-12; <https://doi.org/10.1155/2021/2204776>
- [39] T. Prasad, E. Elumalai, *Asian Pacific Journal of Tropical Biomedicine*, 2011, 1, 439-442; [https://doi.org/10.1016/S2221-1691\(11\)60096-8](https://doi.org/10.1016/S2221-1691(11)60096-8)
- [40] M. S. Alwhibi, D. A. Soliman, M. A. Awad, A. B. Alangery, H. Al Dehaish, Y. A. Alwasel, *Green Processing and Synthesis*, 2021, 10, 412-420; <https://doi.org/10.1515/gps-2021-0039>
- [41] N. AlMasoud, H. Alhaik, M. Almutairi, A. Houjak, K. Hazazi, F. Alhayek, S. Aljanoubi, A. Alkhaibari, A. Alghamdi, D. A. Soliman, *Green Processing and Synthesis*, 2021, 10, 518-528; <https://doi.org/10.1515/gps-2021-0048>
- [42] T. S. Alomar, N. AlMasoud, M. A. Awad, M. F. El-Tohamy, D. A. Soliman, *Materials Chemistry and Physics*, 2020, 249, 123007; <https://doi.org/10.1016/j.matchemphys.2020.123007>
- [43] P. Moteriya, S. Chanda, *Journal of Inorganic and Organometallic Polymers and Materials*, 2020, 30, 3920-3932; <https://doi.org/10.1007/s10904-020-01532-7>
- [44] M. Danaei, M. Dehghankhold, S. Ataei, F. Hasanzadeh Davarani, R. Javanmard, A. Dokhani, S. Khorasani, M. Mozafari, *Pharmaceutics*, 2018, 10, 57; <https://doi.org/10.3390/pharmaceutics10020057>
- [45] A. Suriya, M. Sadiq, G. Munuswamy-Ramanujam, A. Maruthapillai, *Materials Today: Proceedings*, 2022, 68, A1-A6; <https://doi.org/10.1016/j.matpr.2022.11.113>
- [46] P. Banerjee, M. Satapathy, A. Mukhopahayay, P. Das, *Bioresources and Bioprocessing*, 2014, 1, 1-10; <https://doi.org/10.1186/s40643-014-0003-y>
- [47] E. Ajayi and A. Afolayan, *Advances in Natural Sciences: Nanoscience and Nanotechnology*, 2017, 8, 015017; <https://doi.org/10.1088/2043-6254/aa5cf7>
- [48] H. M. Ibrahim, *Journal of radiation research and applied sciences*, 2015, 8, 265-275; <https://doi.org/10.1016/j.jrras.2015.01.007>
- [49] K. Varghese Alex, P. Tamil Pavai, R. Rugmini, M. Shiva Prasad, K. Kamakshi, K. C. Sekhar, *ACS omega*, 2020, 5, 13123-13129; <https://doi.org/10.1021/acsomega.0c01136>
- [50] N. Mohamed, H. El-Masry, *Journal of Nanoanalysis*, 2020, 7, 73-82.
- [51] M. Yamanaka, K. Hara, J. Kudo, *Applied and environmental microbiology*, 2005, 71, 7589-7593; <https://doi.org/10.1128/AEM.71.11.7589-7593.2005>
- [52] F. A. Qais, A. Shafiq, H. M. Khan, F. M. Husain, R. A. Khan, B. Alenazi, A. Alsalme, I. Ahmad, *Bioinorganic chemistry and applications*, 2019, 2019.
- [53] S. Mahalingam, P. K. Govindaraji, V. G. Solomon, H. Kesavan, Y. D. Neelan, S. Bakthavatchalam, J. Kim, P. Bakthavatchalam, *ACS omega*, 2023, 8, 11923-11930; <https://doi.org/10.1021/acsomega.2c07531>
- [54] P. Dibrov, J. Dzioba, K. K. Gosink, C. C. Häse, *Antimicrobial agents and chemotherapy*, 2002, 46, 2668-2670; <https://doi.org/10.1128/AAC.46.8.2668-2670.2002>
- [55] S. Patil, R. Chandrasekaran, *Journal of Genetic Engineering and Biotechnology*, 2020, 18, 1-23; <https://doi.org/10.1186/s43141-020-00081-3>
- [56] S. Shrivastava, T. Bera, A. Roy, G. Singh, P. Ramachandrarao, D. Dash, *Nanotechnology*, 2007, 18, 225103; <https://doi.org/10.1088/0957-4484/18/22/225103>
- [57] Ghosvandi, S., Madani, M., Karimi, J., *Journal of Inorganic and Organometallic Polymers and Materials*, 30, 2020, 2987-2997; <https://doi.org/10.1007/s10904-020-01449-1>